Supplemental figures and legends for

Adipose extracellular vesicle CFD in growth hormone–driven insulin-dependent hepatic steatosis

Peng Wei[1,2,4], Junliang Chen[1,2,4], Tong Wu[2,4], Chengying Xu[2], Yajie Wang[2], Yingjie Zhang[2], Kejian Wei[2], Fei Gao[2], Longlong Wang[2], Guocai Duan[2], Rui Zhao[2], Chuang Liu[2], Tao Wan[1,2,*], Zhonghua Lu[3,*], Fei Fang[1,2,5,*]

[1]Affiliated Hospital of Jiangnan University, Wuxi 214122, China

[2]Wuxi School of Medicine, Jiangnan University, Wuxi 214122, China

[3]Department of Infectious Diseases, Affiliated Hospital of Nantong University, Nantong, Jiangsu 226001, China

[4]These authors contributed equally

[5]Lead contract

*Correspondence: 8202304002@jiangnan.edu.cn, Lu_z_h@126.com, feifang@jiangnan.edu.cn

Address for lead contract:

Fei Fang, Ph.D., Wuxi School of Medicine, Jiangnan University, 1800 Lihu Road, Wuxi 214122, China.

Fig S1

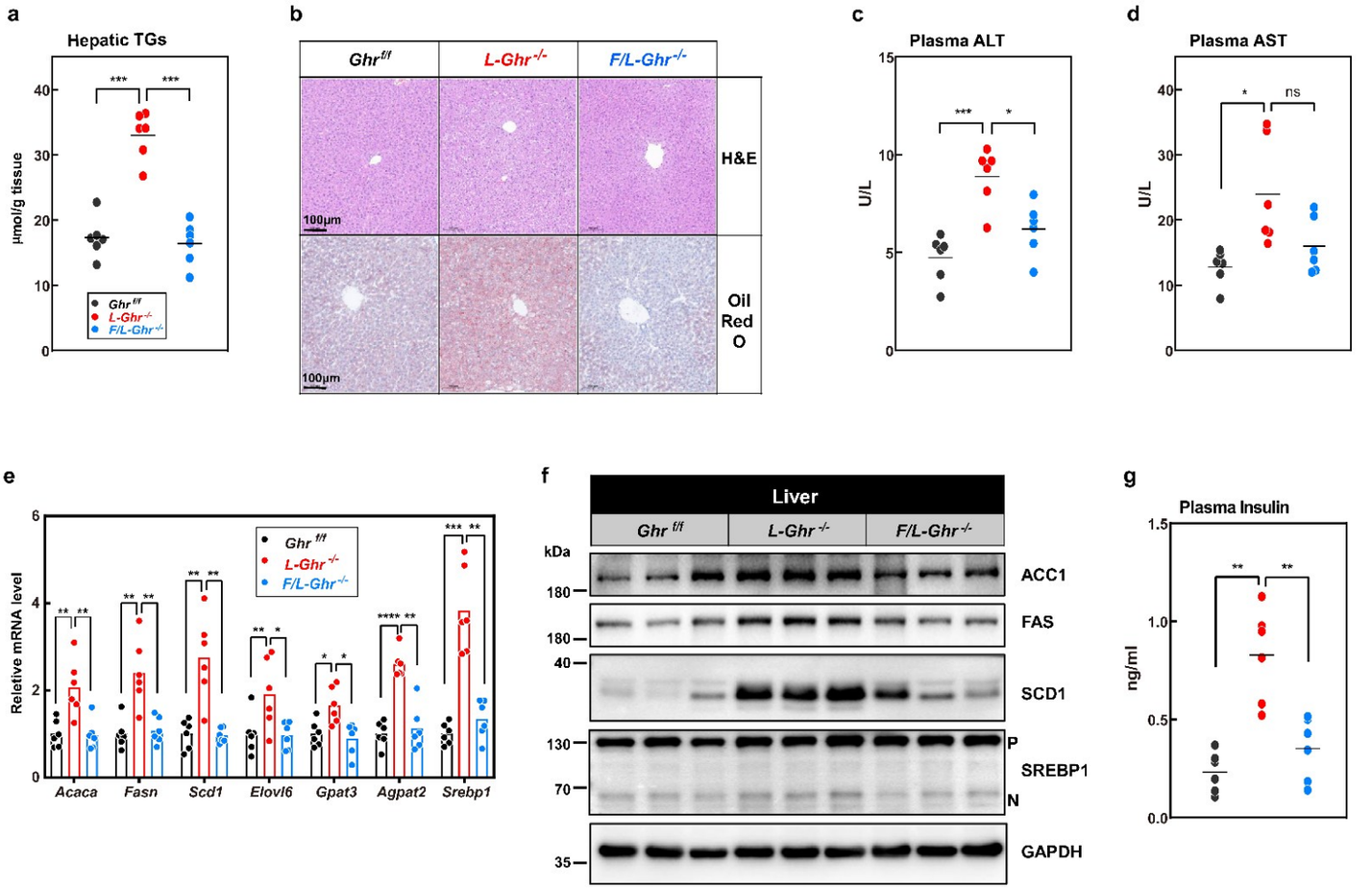


Figure S1. Comparison of hepatic lipogenesis and steatosis in female among *Ghr*$^{f/f}$, *L-Ghr*$^{-/-}$, and *F/L-Ghr*$^{-/-}$ *mice.*

a Hepatic TGs content in liver tissues from female *Ghr*$^{f/f}$, *L-Ghr*$^{-/-}$, and *F/L-Ghr*$^{-/-}$ mice. n=6/group. **b** Representative histological images of mouse liver sections stained with H&E and Oil Red O. n=4/group. Scale bar, 100 μm. **c** Plasma ALT levels in mice of the three genotypes. n=6/group. **d** Plasma AST levels in mice of the three genotypes. n=6/group. **e** RT-qPCR analysis of key lipogenic genes in liver tissue from the mice of the three genotypes. n=6/group. **f** Immunoblot analysis of lipogenic proteins in liver lysates from mice of the three genotypes. n=3 for representative samples. **g** Plasma insulin levels in mice of the three genotypes.

Data (a, c-e, g) are presented as individual values with the means. p values were determined by one-way ANOVA with Tukey's post hoc test. *p < 0.05; **p < 0.01; ***p <0.001; ****p < 0.0001; ns denotes no significance.

Fig S2

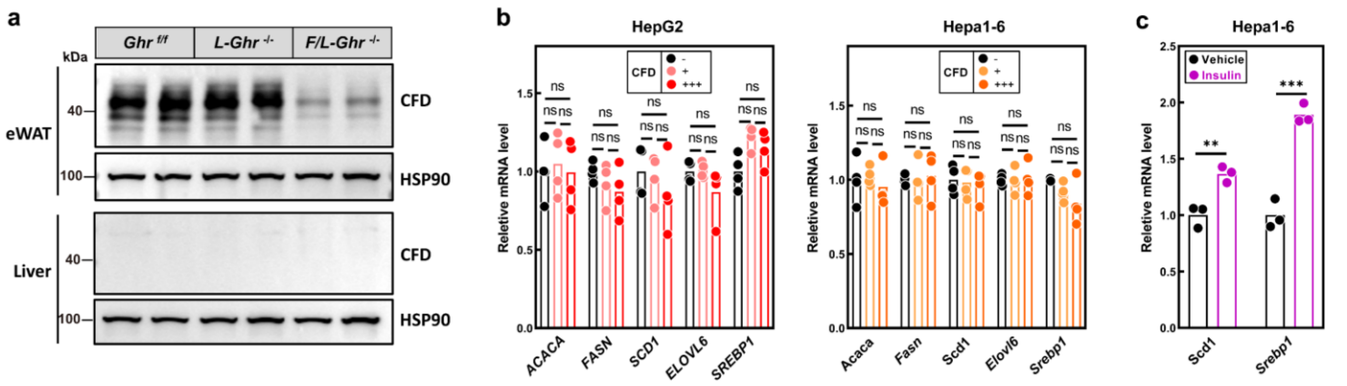


Figure S2. CFD expression in mouse eWAT versus liver, and the effect of CFD on hepatocyte lipogenesis compared with insulin treatment.

a Immunoblot analysis of CFD protein in eWAT and livers from *Ghr*$^{f/f}$, *L-Ghr*$^{-/-}$, and *F/L-Ghr*$^{-/-}$ mice. n=2 for representative samples. **b** RT-qPCR analysis of lipogenic genes expression in HepG2 (left) and Hepa1-6 (right) cells treated with increasing doses of CFD protein. n=4/group. **c** RT-qPCR analysis of *Scd1* and *Srebp1* mRNA levels in Hepa1-6 cells under insulin treatment. n=3/group. Data (b-c) are presented as individual values with the means. p values were determined by one-way ANOVA with Tukey's post hoc test (b), and unpaired Student's t test (c). **p < 0.01; ***p <0.001; ns denotes no significance.

Fig S3

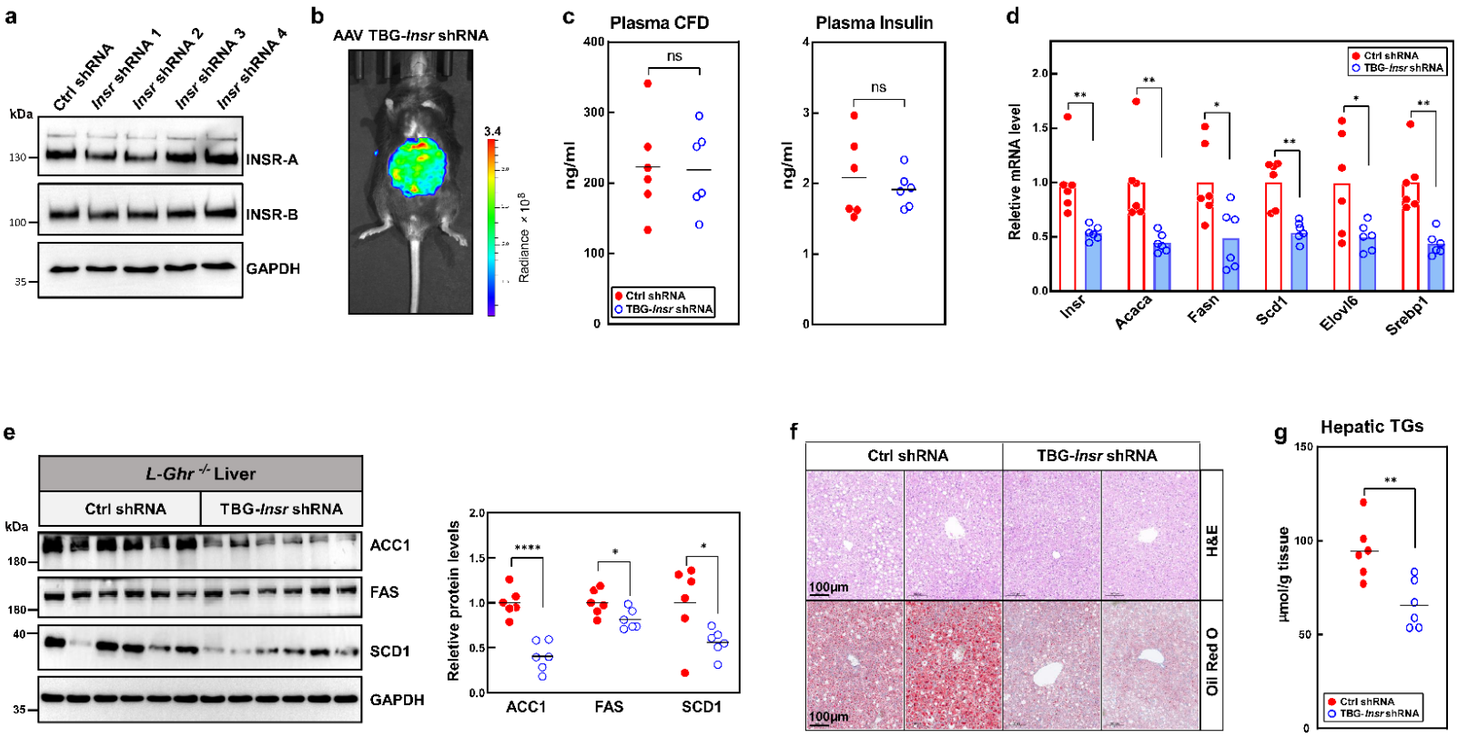


Figure S3. Hepatic insulin receptor knockdown reduces lipid accumulation in *L-Ghr* $^{-/-}$ mice.

a Immunoblot analysis validating the knockdown efficiency of INSR-A and INSR-B in Hepa1-6 cells transfected with different shRNA sequences. **b** Representative *in vivo* fluorescence images of *L-Ghr* $^{-/-}$ mice after i.v. injection of AAV-TBG-shRNA, confirming liver-specific transduction. **c** Plasma CFD (left) and plasma insulin (right) levels in *L-Ghr* $^{-/-}$ mice injected with either AAV-TBG control shRNA (Ctrl shRNA) or *insulin receptor* shRNA (*Insr* shRNA). n=6/group. **d** RT-qPCR analysis of hepatic gene expressions in *L-Ghr* $^{-/-}$ mice injected with AAV expressing Ctrl shRNA or *Insr* shRNA. n=6/group. **e** Immunoblot analysis of lipogenic proteins (ACC1, FAS and SCD1) in liver lysates. Relative protein abundance was quantified by ImageJ. n=6 for representative samples. **f** Representative images of H&E and Oil-Red-O staining of liver sections from Ctrl shRNA or *Insr* shRNA injected *L-Ghr* $^{-/-}$ mice. n=4/group. Scale bar, 100 μm. **g** Hepatic TGs content in the same mice. n=6/group. Data (c-e, g) are presented as individual values with the means. p values were determined by unpaired Student's t test. *p < 0.05; **p < 0.01; ****p < 0.0001; ns denotes no significance.

Fig S4

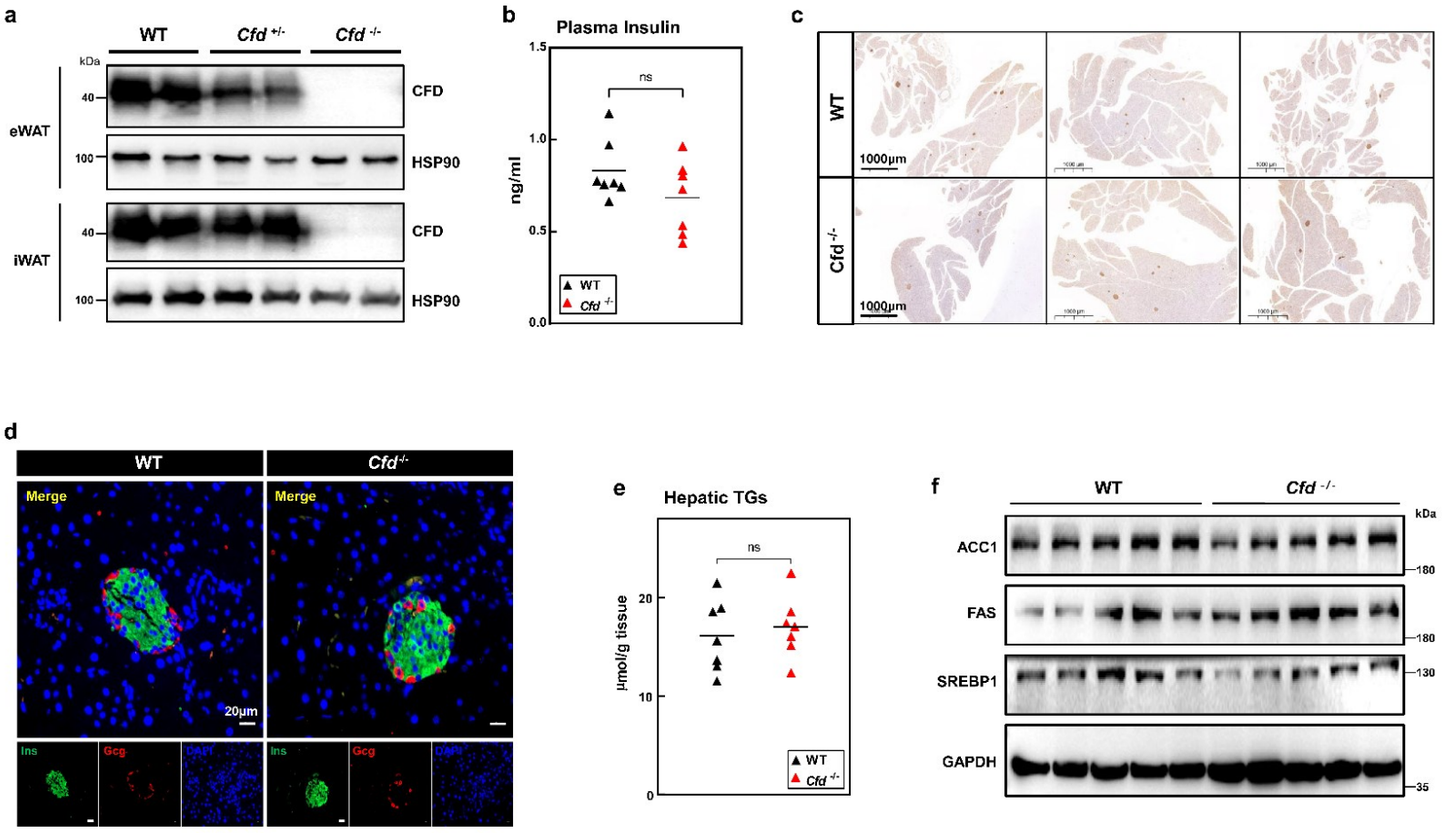


Figure S4. *Cfd* $^{-/-}$ mice on normal diet show no significant differences from WT controls.

a Immunoblot analysis of CFD expression in eWAT and iWAT from WT, *Cfd* $^{+/-}$, and *Cfd* $^{-/-}$ mice fed a normal chow diet. n=2 for representative samples. **b** Plasma insulin levels in chow-fed WT and *Cfd* $^{-/-}$ mice. n=7/group. **c** Representative images of insulin immunohistochemistry in pancreatic sections from chow-fed WT and *Cfd* $^{-/-}$ mice. n=3/group. Scale bar, 1000 μm. **d** Representative immunofluorescent images of pancreatic islets from chow-fed WT and *Cfd* $^{-/-}$ mice, showing insulin (green), glucagon (red), and DAPI (blue). n=3/group. Scale bar, 20 μm. **e** Hepatic TGs content in chow-fed WT and *Cfd* $^{-/-}$ mice. n=7/group. **f** Immunoblot analysis of lipogenic proteins (ACC1, FAS and SREBP1) in livers from WT and *Cfd* $^{-/-}$ mice. n=5 for representative samples. Data (b, e) are presented as individual values with the means. p values were determined by unpaired Student's t test. ns denotes no significance.

Fig S5

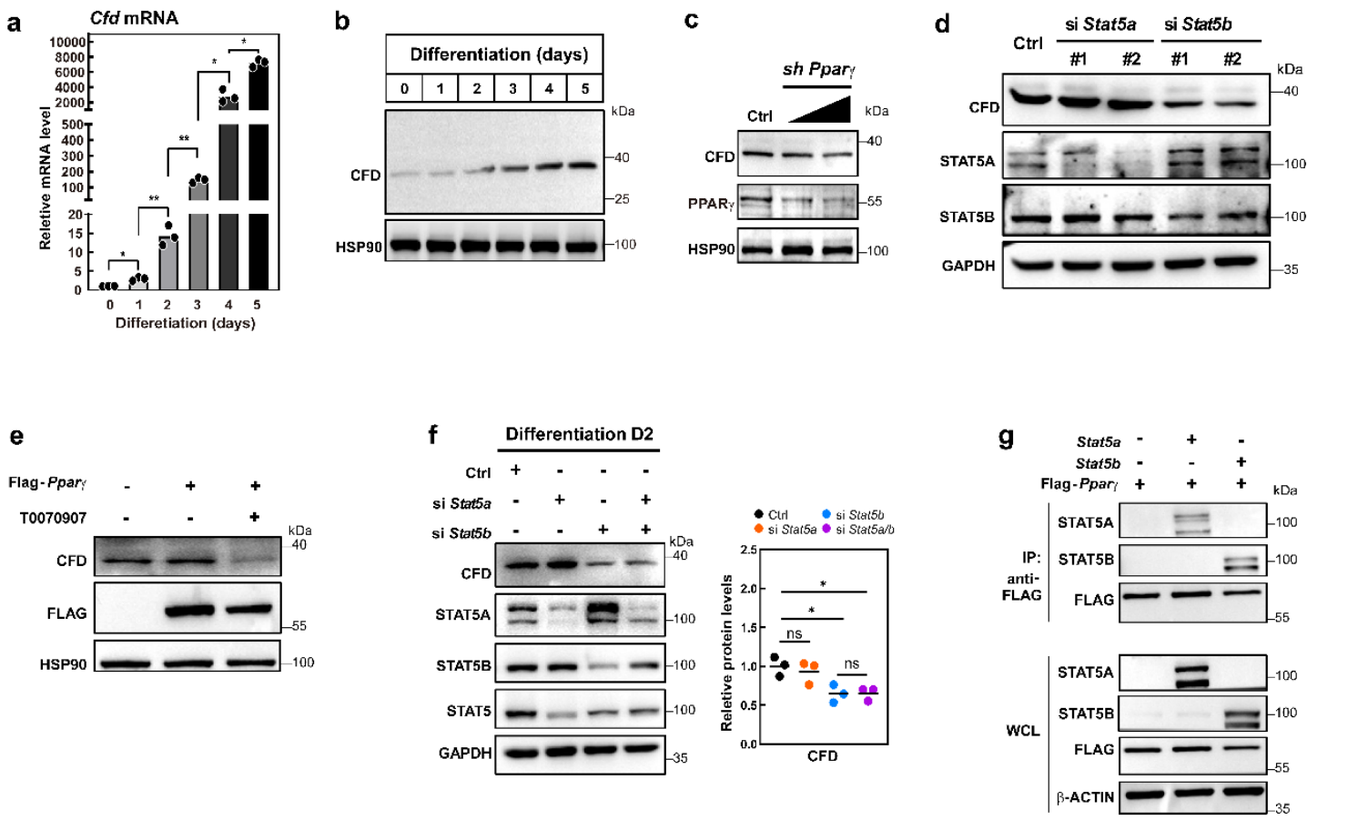


Figure S5. PPAR-γ/STAT5 regulation of CFD in 3T3-L1 adipocytes.
a RT-qPCR analysis of *Cfd* mRNA expression during a time course of 3T3-L1 differentiation from day 0 to day 5. n=3/group. **b** Immunoblot analysis of CFD protein levels during 3T3-L1 differentiation (days 0–5). **c** Immunoblot validation of *Pparγ* shRNA-mediated PPARγ knockdown in 3T3-L1 cells. **d** Immunoblot analysis of CFD expression following siRNA-mediated knockdown of STAT5A or STAT5B in differentiated 3T3-L1 adipocytes. **e** Immunoblot analysis of CFD expression in 3T3-L1 adipocytes overexpressing PPARγ, with or without T0070907 treatment. **f** Immunoblot analysis of CFD, STAT5A, and STAT5B protein levels in differentiated 3T3-L1 adipocytes after siRNA-mediated knockdown of STAT5A or/and STAT5B. CFD protein levels were quantified using ImageJ. n=3 independent experiments. **g**. Co-IP analysis of the PPARγ–STAT5A/B interaction in 3T3-L1 cells overexpressing both PPARγ and STAT5A/B.
Data (f) are presented as individual values with the means. p values were determined by one-way ANOVA with Tukey's post hoc test. *$p < 0.05$; ns denotes no significance.

Fig S6

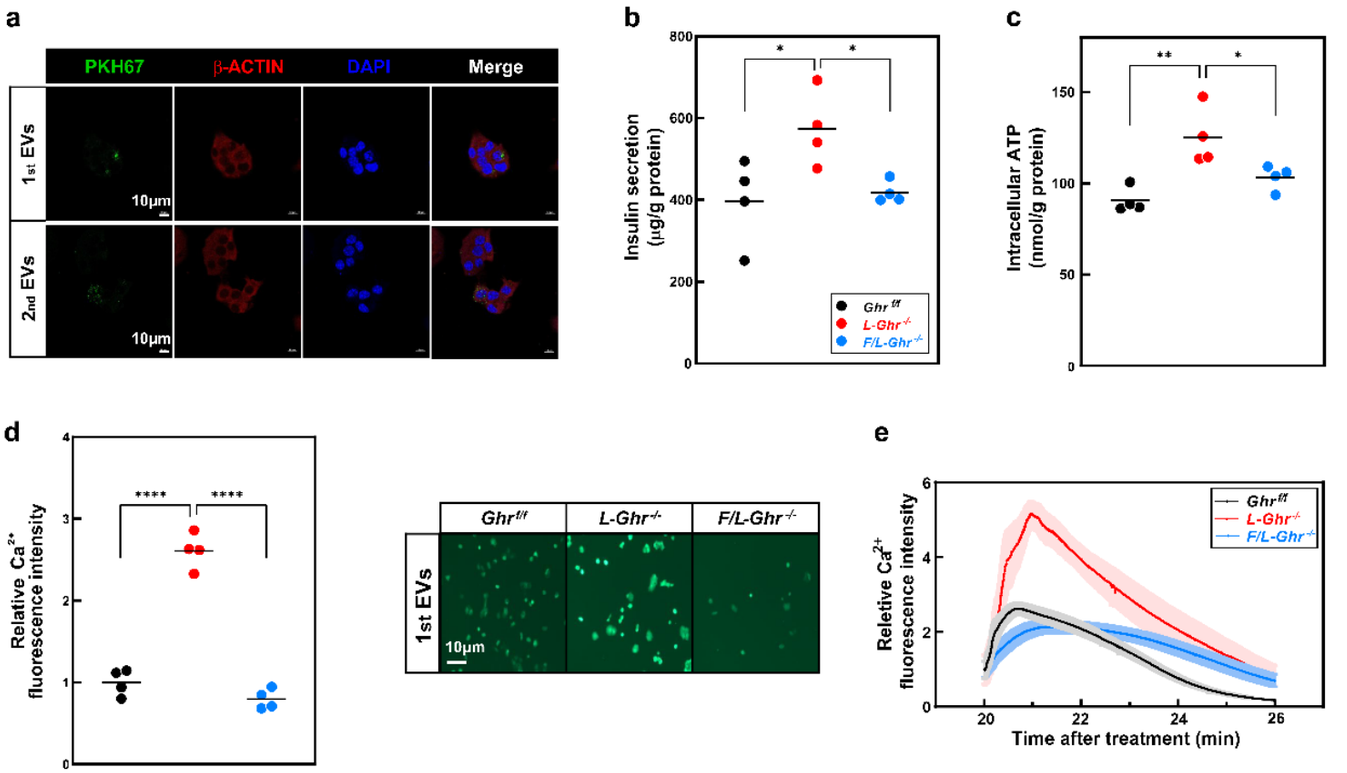


Figure S6. Islet β cell line responses to plasma EVs from *Ghr*$^{f/f}$, *L-Ghr*$^{-/-}$, and *F/L-Ghr*$^{-/-}$ *mice*.

a Immunofluorescence images showing uptake of PKH67-labeled EV fractions (green) by β-TC6 cells; β-actin (red) and DAPI (blue) counterstaining. Scale bar, 10 μm. **b** GSIS assay in β-TC6 cells treated with 1st EVs isolated from plasma of *Ghr*$^{f/f}$, *L-Ghr*$^{-/-}$, and *F/L-Ghr*$^{-/-}$ mice. n=4/group. **c** Intracellular ATP levels in β-TC6 cells under the same treatment as in (b). n=4/group. **d** Intracellular-calcium measurements and immunofluorescence images of β-TC6 cells under the same treatment as in (b). n=4/group. Scale bar, 10 μm. **e** Glucose (16.8 mM)-induced Ca^{2+} influx in β-TC6 cells after stimulation with EVs from *Ghr*$^{f/f}$, *L-Ghr*$^{-/-}$, and *F/L-Ghr*$^{-/-}$ mice. Data are presented as means ± SEM. n=6/group.

Data (b-d) are presented as individual values with the means. p values were determined by one-way ANOVA with Tukey's post hoc test. *$p < 0.05$; **$p < 0.01$; ****$p < 0.0001$.

Fig S7

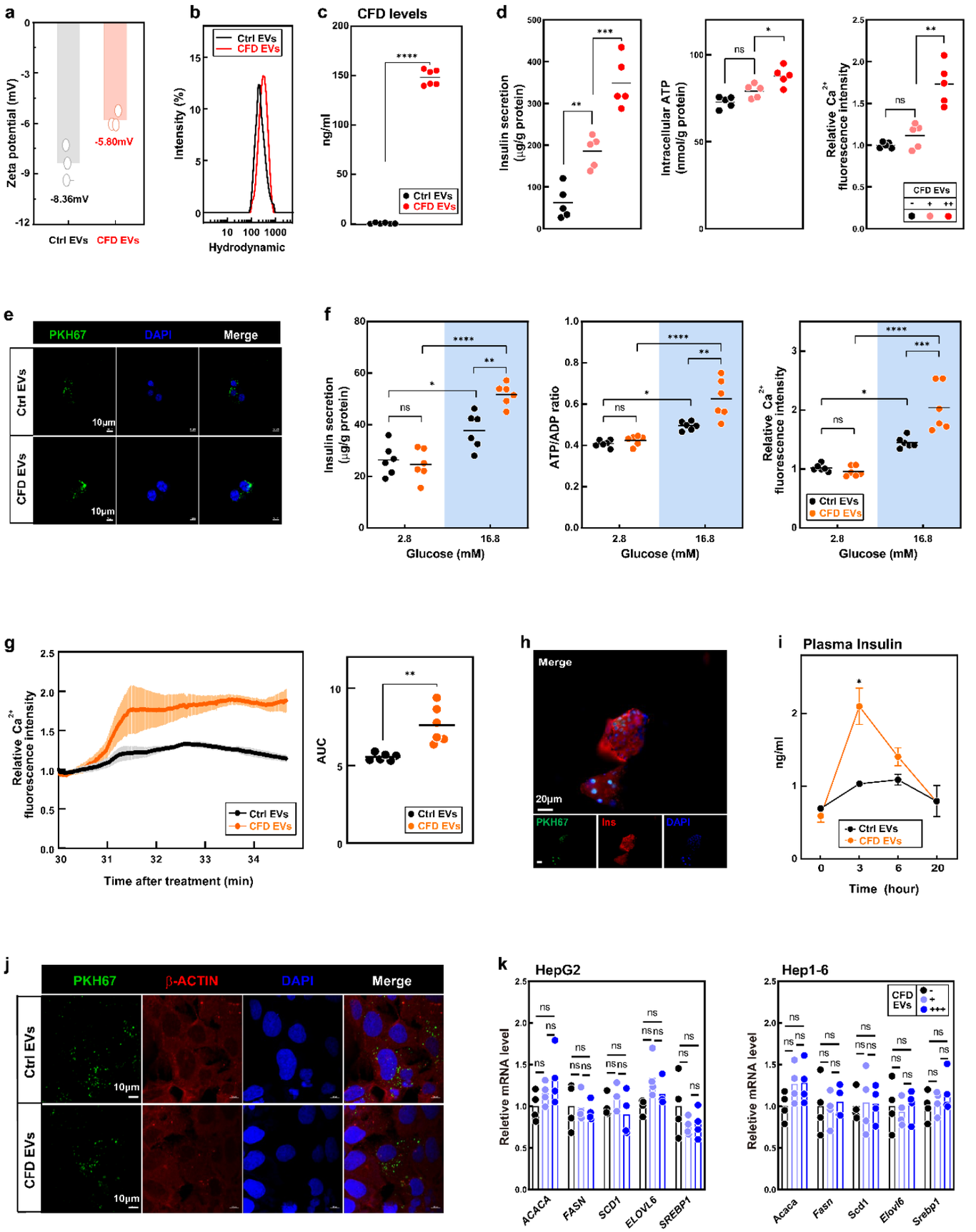

a
Zeta potential (mV)
-8.36mV
-5.80mV
Ctrl EVs
CFD EVs
b
Ctrl EVs
CFD EVs
Intensity (%)
Hydrodynamic
c
CFD levels
ng/ml
Ctrl EVs
CFD EVs
d
Insulin secretion (μg/g protein)
Intracellular ATP (nmol/g protein)
Relative Ca2+ fluorescence intensity
CFD EVs
e
PKH67
DAPI
Merge
Ctrl EVs
CFD EVs
10μm
f
Insulin secretion (μg/g protein)
ATP/ADP ratio
Relative Ca2+ fluorescence intensity
Glucose (mM)
Ctrl EVs
CFD EVs
g
Relative Ca2+ fluorescence intensity
Time after treatment (min)
AUC
h
Merge
20μm
PKH67
Ins
DAPI
i
Plasma Insulin
ng/ml
Time (hour)
Ctrl EVs
CFD EVs
j
PKH67
β-ACTIN
DAPI
Merge
Ctrl EVs
CFD EVs
10μm
k
HepG2
Hep1-6
Reletive mRNA level
CFD EVs
ACACA
FASN
SCD1
ELOVL6
SREBP1
Acaca
Fasn
Scd1
Elovl6
Srebp1

Figure S7. Effects of CFD-loaded EVs on pancreatic islets and hepatocytes.
a Zeta-potential measurement of control EVs (Ctrl EVs) and CFD-loaded EVs (CFD EVs). n=3/group. **b** The hydrodynamic size distribution of Ctrl EVs and CFD EVs. **c** ELISA-based quantification of CFD protein levels in Ctrl EVs and CFD EVs. n=6/group. **d** GSIS, ATP and intracellular-calcium measurements in β-TC6 cells treated with increasing dose of CFD EVs under high-glucose (16.8 mM) condition. n=5/group. **e** Immunofluorescence staining of Min6 cells incubated with PKH67-labeled CFD-loaded EVs (green). DAPI was used for nuclear staining (blue). Scale bar, 10 μm. **f** GSIS, ATP/ADP ratio and intracellular-calcium measurements in Min6 cells incubated with Ctrl EVs and CFD EVs. n=6/group. **g** Glucose (16.8 mM)-induced Ca^{2+} influx in 1.1B4 cells stimulated by Ctrl EVs or CFD EVs, and AUC was quantified. Data are presented as means ± SEM. n=6/group. **h** Representative immunofluorescence images showing the uptake of PKH67-labeled EVs (green) by pancreatic islets in mouse pancreatic tissue after pancreatic ductal infusion. Scale bar, 20 μm. **i** Time-course measurement of plasma insulin levels in mice after pancreatic ductal infusion of Ctrl EVs or CFD EVs. Data are presented as means ± SEM. n=3/group. **j** Immunofluorescence images showing uptake of PKH67-labeled Ctrl EVs or CFD EVs (green) in HepG2 cells; β-actin (red) and DAPI (blue) counterstaining. Scale bar, 10 μm. **k** RT-qPCR analysis of lipogenic gene expression in HepG2 and Hepa1-6 cells treated with increasing dose of CFD EVs. n=4/group.
Data (a, c-d, f, k) are presented as individual values with the means. p values were determined by unpaired Student's t test (a, c, g), and one-way ANOVA with Tukey's post hoc test (d, k), and two-way ANOVA followed by Bonferroni's post hoc test (f, i). *$p < 0.05$; **$p < 0.01$; ***$p < 0.001$; ****$p < 0.0001$; ns denotes no significance.